

Single image dehazing in inhomogeneous atmosphere

Zhenwei Shi^{a,*}, Jiao Long^a, Wei Tang^a, Changshui Zhang^b

^a*Image Processing Center, School of Astronautics, Beihang University, Beijing, China*

^b*Department of Automation, Tsinghua University, Beijing, China*

Abstract

In hazy days, the contrast is reduced with the distance, which hinders the outdoor surveillance system from working properly. Considering the variation of aerosols concentration in inhomogeneous atmosphere and the relation between the attenuation coefficient and aerosols, we propose a more valid model for the attenuation coefficient than the existing one. In this paper, we propose an effective and robust algorithm based on dark channel prior and our optical model in inhomogeneous atmosphere to remove the haze effect from a single input image. In the proposed approach, we refine the coarse transmission map using guided filter, which is very effective while achieving fast speed. Based on our automatically sky region detection, we adjust the refined transmission, with which we can effectively overcome the color distortion in sky regions similar to the atmospheric light. We demonstrate that our method yields similar or even better results than the state-of-the-art techniques while performing fast. Moreover, our simple technique can be applied to most scenes plagued by haze and achieves visually compelling results.

Keywords: Image dehazing, Dark channel, Guided filter, Automatic sky detector.

1. Introduction

In foggy and hazy days, light reflected from an object is scattered and absorbed due to the substantial presence of molecules and aerosols suspended in the atmosphere. With the deterioration of the air quality, haze phenomenon

*Corresponding author. Tel.: +86-10-823-39-520; Fax: +86-10-823-38-798.

Email address: shizhenwei@buaa.edu.cn (Zhenwei Shi)

frequently occurs. Most Chinese cities have witnessed an increasing occurrence of haze in recent years. Due to the effect of dense haze, the transparency of the atmosphere and the visibility are reduced significantly, which will cause considerable disruption to traffic and people's daily lives. Persistent haze obscures the view, making the vehicles, cyclists, and pedestrians move slowly, which often leads to massive traffic jams. In this paper, instead of exploring how to completely wipe out the haze effect from the weather, we focus our attention on how to perfectly remove haze from single hazy images.

In haze weather, images taken in outdoor environment will be severely degraded. Such degraded images are often characterized by poor contrast and low vividness of the scene. The degradation of outdoor images significantly influences the reliability of outdoor vision applications, such as video-surveillance systems, traffic monitoring system and intelligent vehicle. The existence of haze imposes a challenging problem in algorithms that designed for images captured in clear weather. On the other hand, weather is affected by haze at an increasing rate. Moreover, the image dehazing algorithm can also be applied to images captured in underwater environments [1]. Therefore, it is urgent and significant to find an effective algorithm to remove the haze effect from images.

The effect of haze increases with the distance, which makes image dehazing a quite challenge problem. Several researchers have been working on methods of haze removal and proposed several methods by using multiple images. In [2][3][4], a haze-free image is recovered using two or more images of the same scene taken under different weather conditions. By using multiple polarization-filtered images taken at different orientations of the polarizing filter [5][6], the effects of haze can be successfully removed from hazy images. Since our goal is to remove the effects of haze from a single image, such multiple images based techniques are not applicable for our needs.

Widespread attention has been paid to remove haze effects from a single hazy image. Recently, several successful methods for single image dehazing have been proposed. Tan [7] removes haze based on an observation that clear-day images have more contrast than hazy images. The contrast is greatly enhanced, while the recovered images are mostly oversaturated and even deviate from the scene's original colors. Moreover, this algorithm could produce halo artifacts at depth discontinuities. Fattal [8] assumes that the surface shading and medium transmission are locally statistically uncorrelated, and recovers haze-free scene contrast. This approach is physically sound and the recovered results are visually appealing, but it could be invalid when the haze

is thick or the assumption fails. By observing the characteristics of outdoor haze-free images, He et al. [9] propose a dark channel prior, with which dehazing operation can be easily carried out. Although the results obtained by these methods seem visually compelling, their processing speeds are all slow, which hinders surveillance systems from proper functioning. In addition, the attenuation coefficient in these methods is assumed to be constant, while in the actual atmosphere, it changes as a function of altitude, which we will discuss later.

In the present work, we propose an effective and robust algorithm for image dehazing which is based on dark channel prior, originally proposed by He et al. [9]. In most cases, He et al. [9] can recover high-quality haze-free images. However, it could fail when processing haze images containing scene objects similar to the atmospheric light. Color distortions appear in sky regions similar to the atmospheric light. Besides, the recovered results contain halo artifacts in abrupt depth discontinuities. This lies in their haze imaging model, which assumes the attenuation coefficient is constant. Yet in the actual atmosphere, the attenuation coefficient is not a constant but varies with altitude. In this paper, considering changes of the attenuation coefficient, we first present an optical model in inhomogeneous atmosphere. To satisfy this optical model, we adjust the transmission with some strategy. Thus, we are able to handle the color distortions in sky regions and produce high-quality recovered results. Contributions of our paper include:

- (1) We take the inhomogeneous atmosphere into consideration and propose a new model for the attenuation coefficient in the inhomogeneous atmosphere, which differs from the constant attenuation coefficient generally assumed in homogeneous atmosphere.
- (2) In order to get the physically valid transmission, we first propose a simple but effective approach to roughly detect the sky regions, taking advantage of the dark channel images of the original hazy images.
- (3) With the estimated sky region, we adjust the refined transmission. Our adjusted transmission describes the optical model in inhomogeneous atmosphere more accurately. Therefore, we are able to overcome the color distortion in sky regions similar to the atmosphere light and greatly enhance the image contrast.

The remaining of the paper is organized as follows. In Section 2, a detailed analysis of optical model is introduced. The method of our image dehazing algorithm is described in Section 3. Experimental results and evaluation are shown in Section 4. Finally, in Section 5, we conclude the paper and discuss

some possible future work.

2. Background

2.1. Optical model in homogenous atmosphere

The widely used optical model in computer vision and computer graphics [2] [9] [10] is as follows

$$\mathbf{I}(\mathbf{x}) = \mathbf{J}(\mathbf{x})t(\mathbf{x}) + \mathbf{A}(1 - t(\mathbf{x})). \quad (1)$$

Here, $\mathbf{I}(\mathbf{x})$ represents the observed intensity at a pixel $\mathbf{x} = (x, y)$, $\mathbf{J}(\mathbf{x})$ is the original intensity reflected towards the observer from the corresponding scene point, $t(\mathbf{x})$ is the medium transmission which describes the portion of the light that is not scattered and not absorbed and reaches the camera, \mathbf{A} represents the global atmospheric light which is a constant vector. In model (1), both $\mathbf{I}(\mathbf{x})$ and $\mathbf{J}(\mathbf{x})$ have three color channels, and only the input image \mathbf{I} is known. With a single input image \mathbf{I} , we need to estimate the unknowns \mathbf{J} , t , and \mathbf{A} . We can see that image dehazing is essentially an ill-posed problem. Therefore, we need some assumptions or prior knowledge to solve this challenging problem.

According to the optical model (1), the observed intensity at the sensor is contributed by two components, the direct attenuation and airlight [11]. The first term $\mathbf{J}(\mathbf{x})t(\mathbf{x})$ on the right hand of model (1) is called direct attenuation, which describes the scene radiance's attenuation with increasing distance to the observer. The second component is called airlight, which is caused by the scattering of environmental illumination, including direct sunlight, diffuse skylight and light reflected by the ground, by particles suspended in the atmosphere [2]. Airlight is the primary cause of the color shifting, and its expression is $\mathbf{A}(1 - t(\mathbf{x}))$ in model (1).

In a homogeneous atmosphere, the transmission $t(\mathbf{x})$ can be expressed as

$$t(\mathbf{x}) = e^{-\beta d(\mathbf{x})}, \quad (2)$$

where β is the attenuation coefficient [3] due to scattering and absorption, and $d(\mathbf{x})$ represents the distance from the position of pixel \mathbf{x} to the observer. Eq. (2) indicates that the contrast of the scene is reduced exponentially with the distance $d(\mathbf{x})$ increasing. The coefficient β is usually assumed constant in homogeneous medium [2].

2.2. Optical model in inhomogeneous atmosphere

As discussed in Section 2.1, the attenuation coefficient β is considered constant in homogeneous atmosphere. However, the atmospheric medium is not always uniform. Obviously in this situation, the assumption that the attenuation coefficient β is a constant is no longer suitable. In actual atmosphere, the distributions of aerosols are usually not uniform, or rather, they change significantly as a function of altitude. Since the attenuation coefficient β is a result of the scattering properties of the aerosols in the atmosphere, the significant variation in the density of aerosols leads to the change of the attenuation coefficient β [12].

The distributions of aerosols are dominated by gravity, and the density of aerosols presents the exponential decay with the height increasing

$$\rho(h(\mathbf{x})) = \rho_0 e^{-\alpha h(\mathbf{x})}. \quad (3)$$

Here, ρ is the aerosol concentration, ρ_0 is aerosol concentration at earth's surface, α is an exponential attenuation constant, and $h(\mathbf{x})$ represents the height from the pixel \mathbf{x} to the observer.

Since the attenuation coefficient β is proportional to the density of aerosols, the attenuation coefficient also decreases exponentially with respect to height, which can be expressed as

$$\beta(h(\mathbf{x})) = \beta_0 e^{-\alpha h(\mathbf{x})}, \quad (4)$$

where β_0 is the value of attenuation coefficient at earth's surface. According to Eq. (4), the attenuation coefficient $\beta(h(\mathbf{x}))$ in inhomogeneous atmosphere becomes the constant attenuation coefficient β in homogeneous atmosphere when the exponential attenuation constant α is zero. Therefore, the attenuation coefficient model in homogeneous atmosphere is a special case of that in inhomogeneous atmosphere.

According to the definition of the attenuation coefficient in Eq. (4), the attenuation coefficient depends upon the height of objects in the inhomogeneous atmosphere, and a constant attenuation coefficient which is independent of the height is not accurate enough to describe the optical model. In addition, Eq. (4) gives a more accurate description of imaging process in actual atmosphere.

3. Single Image Dehazing in Inhomogeneous Atmosphere

This section investigates single image dehazing in inhomogeneous atmosphere. Our image dehazing work is based on the dark channel prior [9] and

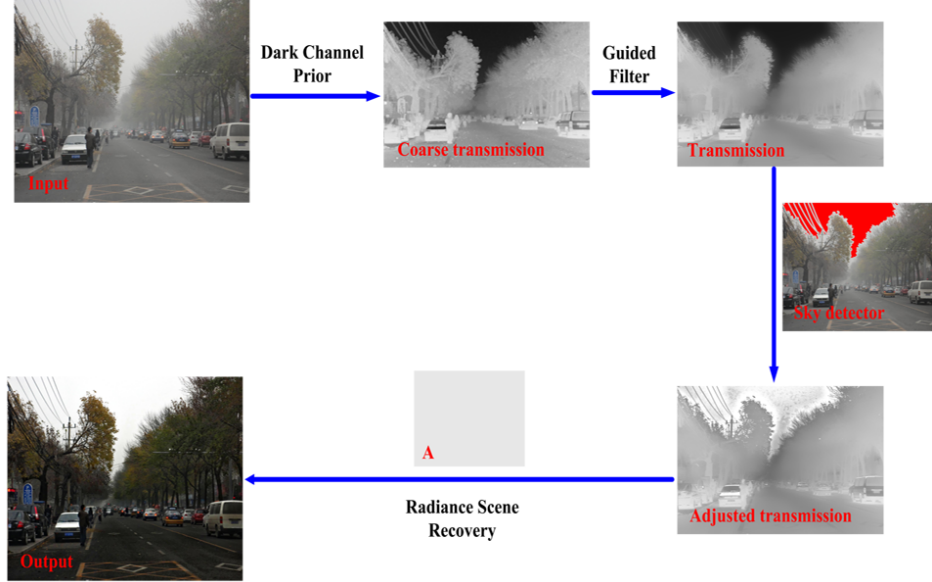


Fig. 1: The framework of our algorithm proposed in this paper. We first estimate the global atmospheric light and calculate the rough transmission map using the dark channel prior, then refine the transmission map with guided filter. In order to solve the color distortion in the sky region, we approximately detect the sky region in the input hazy image and recompute the adjusted transmission map. Finally, we recover the scene radiance with the global atmospheric light and the adjusted transmission map.

the guided filter [13]. The framework of our dehazing algorithm is shown in Fig. 1.

In model (1), obviously, when the transmission $t(\mathbf{x})$ and the global atmospheric light \mathbf{A} are known, the scene radiance $\mathbf{J}(\mathbf{x})$ can be easily calculated by

$$\mathbf{J}(\mathbf{x}) = \mathbf{A} - (\mathbf{A} - \mathbf{I}(\mathbf{x}))/t(\mathbf{x}). \quad (5)$$

In the remaining of this section, we first estimate the global atmospheric light \mathbf{A} . To obtain the transmission $t(\mathbf{x})$, we first get the coarse transmission and refine it with the guided filter, then adjust the refined transmission. Finally, we restore the scene radiance with the global atmospheric light \mathbf{A} and the adjusted transmission $t(\mathbf{x})$.

3.1. Atmospheric Light Estimation

First, we give a description of dark channel prior, which was originally proposed by He et al. [9]. The dark channel prior is discovered based on

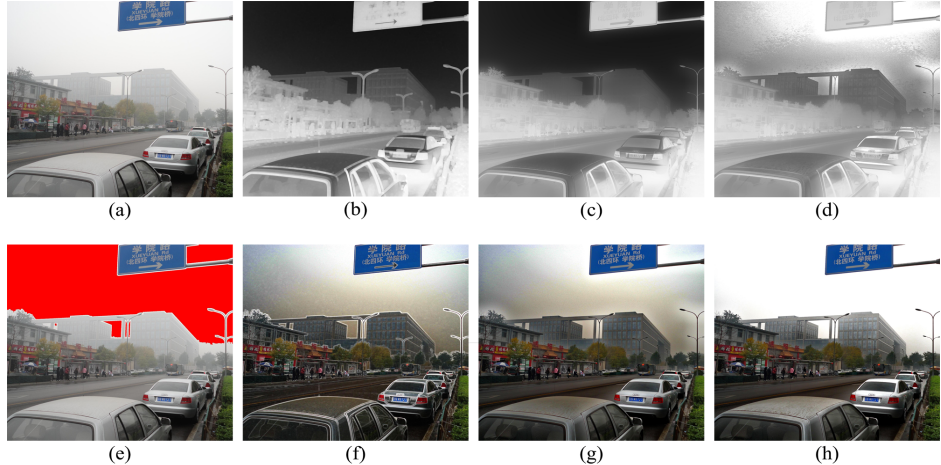


Fig. 2: (a) Input hazy image. (b) Coarse transmission map. (c) Refined transmission map. (d) Our adjusted transmission map. (e) Detected sky region. Red pixels indicate where the sky region is in the hazy image. (f),(g),(h) Recovered images using (b), (c) and (d), respectively.

statistic of observations on 5,000 outdoor haze-free images. In a small local non-sky region, at least one of its RGB channels has very low intensity and is even close to zero, and this is called dark channel prior. For an image \mathbf{J} , its dark channel is defined as

$$J^{dark}(\mathbf{x}) = \min_{\mathbf{y} \in \Omega(\mathbf{x})} (\min_{c \in \{r,g,b\}} J^c(\mathbf{y})), \quad (6)$$

where J^c is a color channel of image \mathbf{J} , $\Omega(\mathbf{x})$ is a local patch centered at \mathbf{x} . According to dark channel prior [9], for an outdoor haze-free image \mathbf{J} , the intensity of its dark channel image J^{dark} is very low and close to zero except for sky regions.

However, the dark channel prior is not applicable to images taken under haze conditions. Due to the effect of additive airlight, the intensity of pixels in haze regions is high in all color channels, and moreover, the minimal intensity of local area is high as well. Visually, the intensity of the dark channel is a rough approximation of the thickness of the haze [9]. According to this prior information, the global atmospheric light can be easily estimated.

According to the optical model (1), the airlight becomes more dominant with the distance from the object to the observer increasing. As observed by Narasimhan and Nayar [14], the global atmospheric light \mathbf{A} is best estimated

in the most haze-opaque region. As discussed before, a hazy image's dark channel is the approximation of the haze thickness. Therefore, we can easily find the most haze-opaque area in the dark channel of images taken under haze conditions and estimate the global atmospheric light. Since the most haze-opaque region is usually located at the top of an image, we use the first L rows of the image to quickly obtain the global atmospheric light. In our case, the parameter L is fixed at one-twentieth of the input image height. We first cut out the first L rows of the hazy image and calculate its dark channel, then we choose the top 0.1 percent brightest pixels in the dark channel as the most haze-opaque region. In this haze-opaque region, the brightest pixel in the original hazy image is estimated as the global atmospheric light.

3.2. Transmission Estimation and Refinement

With the dark channel prior, the coarse transmission $\tilde{t}(\mathbf{x})$ can be easily obtained by the following equation

$$\tilde{t}(\mathbf{x}) = 1 - \omega \min_{\mathbf{y} \in \Omega(\mathbf{x})} \left(\min_{c \in \{r,g,b\}} \frac{I^c(\mathbf{y})}{A^c} \right), \quad (7)$$

where I^c is a color channel of image \mathbf{I} , $\Omega(\mathbf{x})$ is a local patch centered at \mathbf{x} , and ω is a constant parameter representing a small amount of haze kept for distant objects. A typical value of the parameter ω is 0.95, suggested in [9].

However, as shown in Fig. 2, recovered images (see Fig. 2(f)) using the coarse transmission (see Fig. 2(b)) usually have block artifacts and halos especially in regions with abrupt depth discontinuities. This is because the assumption that the transmission in a local patch is constant is not always true. Therefore, we need to use some strategies to refine the transmission in order to get better recovery results.

In [9], He et al. find that the optical model (1) is similar to the image matting equation, and then apply a closed-form matting framework [15] to refine the transmission $\tilde{t}(\mathbf{x})$. However, although this approach can produce impressive results, it has the disadvantage of solving large-scale linear system, which is very time-consuming.

In this paper, we present a fast method, which is called guided filter [13], to refine the coarse transmission map $\tilde{t}(\mathbf{x})$. The guided filter, derived from a local linear model between the guidance and the filter output, can preserve edges like bilateral filter [16], while having even better performance near the edges. Moreover, the computational complexity of the guided filter

is independent of the filtering kernel size. More specifically, the guided filter is a fast and linear-time algorithm, which can achieve very fast speed. The refined transmission map t is assumed to be a linear transform of the input hazy image \mathbf{I} in a window ω_k centered at the pixel k :

$$t_i = \mathbf{a}_k^T \mathbf{I}_i + b_k, \forall i \in \omega_k, \quad (8)$$

where t_i represents the refined transmission of a pixel i , \mathbf{I}_i is a 3×1 color vector, \mathbf{a}_k is a 3×1 coefficient vector, and b_k is a scalar. The window ω_k is a square window with a side length of r . According to Eq. (8),

$$\nabla t = \mathbf{a}^T \nabla \mathbf{I}, \quad (9)$$

where ∇t means the gradient of t , and $\nabla \mathbf{I}$ means the gradient vector of \mathbf{I} . Eq. (9) indicates that the refined transmission will have an edge if the input image has an edge. In order to maximally reserve the information of the original transmission and minimize the difference between the refined transmission and the coarse one, we minimize the following cost function in window ω_k :

$$E(\mathbf{a}_k, b_k) = \sum_{i \in \omega_k} (\mathbf{a}_k^T \mathbf{I}_i + b_k - \tilde{t})^2. \quad (10)$$

In [13], in order to restrict the range of the length of \mathbf{a}_k , a regulation term is further added in Eq. (10)

$$E(\mathbf{a}_k, b_k) = \sum_{i \in \omega_k} ((\mathbf{a}_k^T \mathbf{I}_i + b_k - \tilde{t})^2 + \epsilon \mathbf{a}_k^T \mathbf{a}_k), \quad (11)$$

where ϵ is a regulation parameter preventing the length of \mathbf{a}_k from being too large.

To solve this optimization problem, we use the linear regression [17], and the solution to Eq. (8) is

$$\mathbf{a}_k = (\Sigma_k + \epsilon U)^{-1} \left(\frac{1}{|\omega|} \sum_{i \in \omega_k} \mathbf{I}_i \tilde{t}_i - \boldsymbol{\mu}_k \bar{\tilde{t}}_k \right), \quad (12)$$

$$b_k = \bar{\tilde{t}}_k - \mathbf{a}_k^T \boldsymbol{\mu}_k, \quad (13)$$

where $\boldsymbol{\mu}_k$ and Σ_k are respectively the mean 3×1 vector and 3×3 covariance matrix of \mathbf{I} in ω_k , $|\omega|$ is the number of pixels in ω_k , U is a 3×3 identity matrix, and $\bar{\tilde{t}}_k = \frac{1}{|\omega|} \sum_{i \in \omega_k} \tilde{t}_i$ is the mean of \tilde{t} in ω_k .

However, the value of t_i calculated with (8) varies in different windows since the pixel i appears in all windows ω_k that contain i . To avoid repeatedly computation and the uncertainty of t_i , we compute the average of all values of t_i :

$$t_i = \frac{1}{|\omega|} \sum_{k:i \in \omega_k} (\mathbf{a}_k^T \mathbf{I}_i + b_k) \quad (14)$$

$$= \bar{\mathbf{a}}_i^T \mathbf{I}_i + \bar{b}_i, \quad (15)$$

where $\bar{\mathbf{a}}_i = \frac{1}{|\omega|} \sum_{k \in \omega_i} \mathbf{a}_k$ and $\bar{b}_i = \frac{1}{|\omega|} \sum_{k \in \omega_i} b_k$.

With Eq. (15), we can easily obtain the refined transmission map. In this situation, $\nabla t \approx \bar{\mathbf{a}} \nabla \mathbf{I}$, which means that abrupt depth discontinuities in input image \mathbf{I} can be mostly maintained in the refined transmission t . Fig. 2(c) shows the refined transmission using the coarse transmission in Fig. 2(b) as a guidance. Fig. 2(c) illustrates that refined transmission preserves the edges in input image and is very smooth without any block artifacts. The corresponding recovered image is shown in Fig. 2(g), from which we can see that the result preserves the very fine details and removes the haze effect thoroughly. However, the color distortion appears in sky regions and some halo artifacts still exist in abrupt depth discontinuities. In order to solve these problems, we further adjust the refined transmission.

3.3. Automatic Sky Detector

Due to the halo artifacts and color distortion in recovered images, which is resulted from the refined transmission obtained by Eq. (15), the results look unnatural. Fig. 2(c) illustrates that the transmission in sky region is dark, which satisfies the definition of transmission in Eq. (2). According to Eq. (2), the transmission decreases with the increasing distance. Therefore, sky regions with infinite distances have low transmission. However, as we discussed in Section 2.2, in inhomogeneous atmosphere, the attenuation coefficient β decreases exponentially with height, which is $\beta(h(\mathbf{x})) = \beta_0 e^{-\alpha h(\mathbf{x})}$. In this situation, the sky region, located at a great distance from the observer, has a low attenuation coefficient near zero, which leads to a high transmission in the sky region. In brief, the refined transmission calculated by Eq. (15) is inconsistent with the physics.

Here, we first propose a simple but effective approach to automatically detect the rough sky region in the input hazy image, based on which we adjust the refined transmission. The method contains two crucial parameters, the

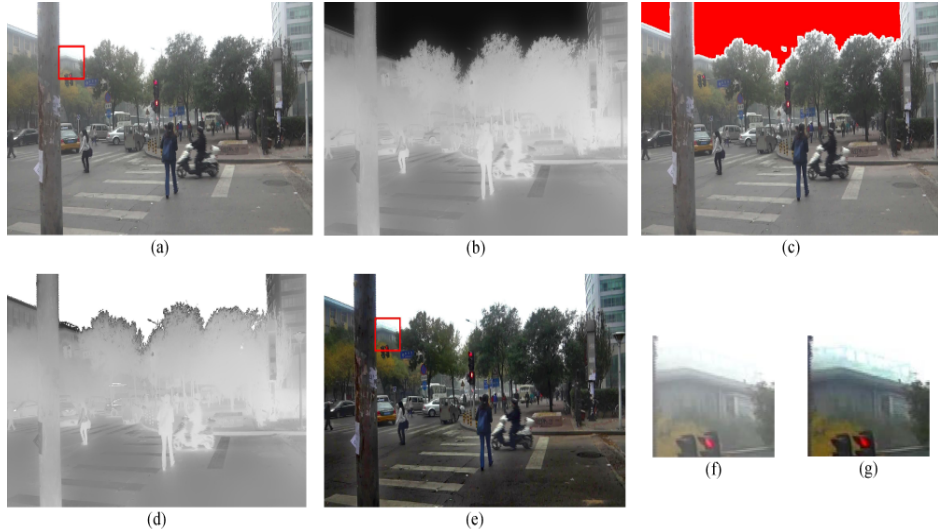


Fig. 3: (a) Input hazy image. (b) Refined transmission map. (c) Detected sky region. (d) Our adjusted transmission map. (e) Our haze removal result. (f), (g) Two patches that are extracted from input hazy image and the recovered image indicated with red rectangles, respectively.

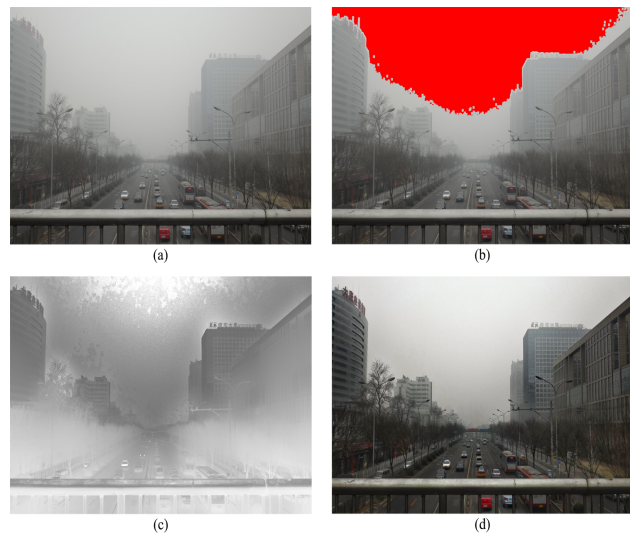


Fig. 4: a) Input hazy image. (b) Detected sky region. (c) Our adjusted transmission map. (d) Our haze removal result.

global atmospheric light \mathbf{A} and the coarse transmission $\tilde{t}(\mathbf{x})$. According to Section 3.1 and Section 3.2, we can easily estimate these parameters.

Obviously, sky regions are most likely to show up at the top of the field of view. In sky regions, the intensity of pixels in all color channels is large, which is close to or even higher than the value of global atmospheric light \mathbf{A} . In addition, according to the coarse transmission obtained using dark channel prior, the transmission in sky regions is low. With all the above constraints, we can roughly estimate the sky region in original hazy image. A pixel \mathbf{x} is assumed to be located in the sky region only if the following set of constraints is true:

$$\begin{cases} x < N, \\ \mathbf{I}(\mathbf{x}) > k\mathbf{A}, \\ \tilde{t}(\mathbf{x}) < l. \end{cases} \quad (16)$$

Here, x represents the row index of input hazy image \mathbf{I} , N , k , and l are all constant parameters. Considering the characteristics of the location of sky regions and their corresponding transmission, the parameters N and l are fixed at two-thirds of the input image height and 0.2, respectively. The parameter k measures the degree of similarity between the atmospheric light and sky regions. In our experiments, we set $k = 0.8$.

Some examples of automatic sky detection are shown in Fig. 2(e), Fig. 3(c), Fig. 4(b), Fig. 5(e), and Fig. 7(c), where the estimated sky regions are marked in red. We can see that our method can detect sky regions effectively. Also, it should be noted that we apply this approach automatically and routinely in all of our experiments. Fig. 6(c) shows another example of the sky region estimation. This figure illustrates that no sky region is detected, which is in accordance with the intuition of Fig. 6(a) (a hazy image containing no sky region at all).

3.4. Scene Radiance Recovery

The scene radiance recovered by the simple refined transmission often contains halo artifacts and color distortions especially in sky regions. With the automatic sky detector, we can solve these problems with ease.

An alternative way to express Eq. (5) is

$$\mathbf{J}(\mathbf{x}) = \frac{\mathbf{I}(\mathbf{x}) - \mathbf{A}}{t(\mathbf{x})} + \mathbf{A}, \quad (17)$$

which indicates that for sky regions whose intensity is lower than the value of global atmospheric light \mathbf{A} , if their corresponding transmission is low at the same time, it is most likely to have color distortion in these areas. More specifically, with the low transmission in sky regions, the difference among the color channels will be magnified several times after dividing this low transmission t even if the intensity of the red channel I^r , the green channel I^g , and the blue channel I^b is very close to each other according to Eq. (17). As a result, the recovered color inevitably deviates from the original scene and the restored haze-free image may look unnatural (please see Fig. 2(g)).

We propose an alternative way to solve these problems. Obviously, the main cause lies in the inaccurate transmission. Regardless of the dark channel prior, the accurate transmission is

$$t_{actual}(\mathbf{x}) = \frac{1 - \min_{\mathbf{y} \in \Omega(\mathbf{x})} (\min_{c \in \{r,g,b\}} \frac{I^c(\mathbf{y})}{A^c})}{1 - \min_{\mathbf{y} \in \Omega(\mathbf{x})} (\min_{c \in \{r,g,b\}} \frac{J^c(\mathbf{y})}{A^c})}. \quad (18)$$

In bright regions such as sky and white objects, $\min_{\mathbf{y} \in \Omega(\mathbf{x})} (\min_{c \in \{r,g,b\}} \frac{J^c(\mathbf{y})}{A^c})$ is large and will not be close to zero, which means that the actual transmission $t_{actual}(\mathbf{x})$ is larger than $t(\mathbf{x})$ estimated by Eq. (15). To satisfy the optical model in inhomogeneous atmosphere, we adjust the refined transmission by the following equation:

$$t'(\mathbf{x}) = \min(\max(M/|\mathbf{I}(\mathbf{x}) - \mathbf{A}|, 1) \cdot t(\mathbf{x}), 1). \quad (19)$$

Here, M is a parameter that thresholds the difference between the color channel of image $\mathbf{I}(\mathbf{x})$ and the global atmospheric light \mathbf{A} . In our case, the threshold M is determined by the relation between the value of the global atmospheric light \mathbf{A} and the intensity of the sky region detected in Section 3.3. If the sky region's intensity is larger than the value of global atmospheric light, the threshold M is constrained to a small value. Otherwise, M is given a large value. In our case, the small and large values of the threshold M are 10 and 80, respectively. Note that, when the threshold M equals zero, the adjusted transmission $t'(\mathbf{x})$ turns to the refined transmission $t(\mathbf{x})$.

Some examples of our adjusted transmission are shown in Fig. 2, Fig. 3, Fig. 4. Fig. 2(d) and 3(d) are the corresponding adjusted transmissions of the refined transmissions shown in Fig. 2(c) and Fig. 3(b), respectively. The difference between the adjusted transmission and the refined one is very



Fig. 5: Comparison with Tan’s work [7]. (a) Input hazy image. (b) Tan’s result. (c) Our result. (d) Refined transmission. (e) Detected sky region. (f) Our adjusted transmission.

obvious. In the sky region, the refined transmission is very low and even close to zero while the adjusted one is high. As we mentioned before, in the actual atmosphere, the transmission in sky regions is high. Therefore, our adjusted transmission is more suitable for describing the optical model in actual atmosphere.

Substituting the refined transmission $t(\mathbf{x})$ with our adjusted transmission $t'(\mathbf{x})$ in Eq. (19), the ultimate recovered scene radiance $\mathbf{J}(\mathbf{x})$ can be restored by

$$\mathbf{J}(\mathbf{x}) = \frac{\mathbf{I}(\mathbf{x}) - \mathbf{A}}{t'(\mathbf{x})} + \mathbf{A}. \quad (20)$$

Some final restored images are shown in Fig. 2, Fig. 3, Fig. 4.

We show our proposed scene radiance restoration algorithm in Algorithm 1.

4. Experimental Results and Evaluation

In order to demonstrate the effectiveness and robustness of our proposed algorithm, we have tested our method on a large set of hazy images in natural environment and urban traffic scene environment. Also, we give several comparisons with the state-of-art algorithms. We claim that our method

Algorithm 1 The scene radiance restoration

Step 1: Input an original hazy image $\mathbf{I}(\mathbf{x})$ and compute the dark channel of the first L rows of \mathbf{I} as

$$I^{dark}(\mathbf{x}) = \min_{\mathbf{y} \in \Omega(\mathbf{x})} (\min_{c \in \{r,g,b\}} I^c(\mathbf{y})), x < L,$$

where x represents the row index of the hazy image.

Step 2: Estimate the global atmospheric light.

Among the top 0.1 percent brightest pixels in the dark channel $I^{dark}(\mathbf{x})$, the brightest pixel in the original image \mathbf{I} is considered as the global atmospheric light \mathbf{A} .

Step 3: Estimate the coarse transmission by

$$\tilde{t}(\mathbf{x}) = 1 - \omega \min_{\mathbf{y} \in \Omega(\mathbf{x})} (\min_{c \in \{r,g,b\}} \frac{I^c(\mathbf{y})}{A^c}).$$

Step 4: Refine the coarse transmission using guided filter:

$$t_i = \bar{\mathbf{a}}_i^T \mathbf{I}_i + \bar{b}_i,$$

where $\bar{\mathbf{a}}_i = \frac{1}{|\omega|} \sum_{k \in \omega_i} \mathbf{a}_k$ and $\bar{b}_i = \frac{1}{|\omega|} \sum_{k \in \omega_i} b_k$, $\mathbf{a}_k = (\Sigma_k + \epsilon U)^{-1} (\frac{1}{|\omega|} \sum_{i \in \omega_k} \mathbf{I}_i \tilde{t}_i - \boldsymbol{\mu}_k \tilde{t}_k)$, $b_k = \tilde{t}_k - \mathbf{a}_k^T \boldsymbol{\mu}_k$.

Step 5: Detect the sky region.

If a pixel \mathbf{x} satisfies the following set of constraints:

$$\begin{cases} x < N, \\ \mathbf{I}(\mathbf{x}) > k\mathbf{A}, \\ \tilde{t}(\mathbf{x}) < l, \end{cases}$$

we consider that the pixel \mathbf{x} belongs to the sky region.

Step 6: Adjust the refined transmission by the following equation

$$t'(\mathbf{x}) = \min(\max(M/|\mathbf{I}(\mathbf{x}) - \mathbf{A}|, 1) \cdot t(\mathbf{x}), 1).$$

Step 7: Restore the scene radiance by

$$\mathbf{J}(\mathbf{x}) = \frac{\mathbf{I}(\mathbf{x}) - \mathbf{A}}{t'(\mathbf{x})} + \mathbf{A}.$$

generates visually appealing results whether the input images contain sky regions or not. Compared with other existing techniques, the superiority of our algorithm is that we are able to enhance the image contrast while retaining the very fine details and preserving the color of the original scene. Our adjusted transmission, which is high in sky regions, is more accurate to describe the imaging process in actual atmosphere than the refined transmission. Therefore, with the adjusted transmission we can nicely handle the sky regions, the restored results of which always have color distortion when recovered using the refined transmission. Another advantage of our algorithm is the computation time. Our method implemented on CPU(3.2GHz Intel Core i5 Processor) processes a 600×400 pixel image in 0.4 seconds. In comparison, the method of Tan [7] needs five to seven minutes to process a 600×400 pixel image and the algorithm of Fattal [8] takes 35 seconds to process a 512×512 pixel image, while the method of He et al. [9] requires 10-20 seconds to process a 600×400 pixel image.

4.1. Qualitative Comparison

Figs. 2, 3 and 4 show sky regions detected in the input hazy images, our adjusted transmission map, and our recovered images. These images are all urban traffic scenes plagued by haze, and Fig. 2 and Fig. 4 are taken in dense haze conditions. The global atmospheric light and sky regions in these images are automatically estimated by our proposed algorithm. As can be seen from these figures, the adjusted transmissions calculated by our proposed algorithm are all high in sky regions, which is consistent with the optical model in the inhomogeneous atmosphere. As illustrated in these figures, sky regions are effectively and robustly detected. In addition, restored results indicate that our method is able to remove the haze effects while retaining very fine details and preserving the color of original scenes. Furthermore, the contrast in these images is greatly enhanced. As can be seen from Fig. 3(f), objects on the roof of the building which can barely be seen by human eye are well restored by our proposed algorithm (please see Fig. 3(g)), and their visibility is greatly improved as well.

In Fig. 5, we compare our method with Tan's work [7]. Tan removes the haze effect by maximizing the local contrast of the recovered image. As can be seen from Fig. 5(b), the color of the recovered image using this method is oversaturated even though the contrast is greatly enhanced. The main reason is that this method is essentially image enhancement technique which is physical invalid in most cases. Our dehazing algorithm can greatly improve

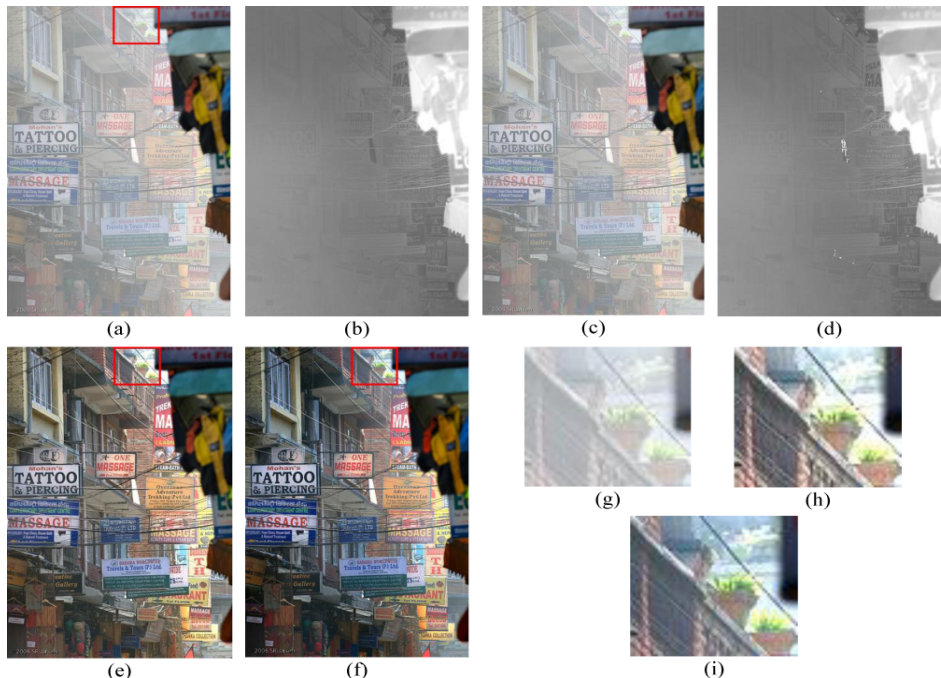


Fig. 6: Comparison with He et al.'s work [18]. (a) Input hazy image. (b) Refined transmission map. (c) Detected sky region. (d) Our adjusted transmission map. (e) He et al.'s result [18]. (f) Our haze removal result. (g), (h), (i) Three patches that are extracted from input hazy image , He et al.'s result [18] and our result indicated with red rectangles, respectively.

the visibility while preserving the original color information as well, which can be seen from Fig. 5(c).

In Fig. 6, we compare our method with He et al.'s work [18]. As can be seen from Fig. 6(g), (h) and (i), He et al.'s recovered result loses some details at the top right of the image. More specifically, the flowers in the original hazy image are restored to be white, which may be overflowed in He et al.'s result. Moreover, plants in pots are kind of wrongly recovered. The loss of color and texture information will lead to enormous loss in important occasions. However, our recovered result can well maintain all the detail information of original hazy image without sacrificing the fidelity of the colors.

Fig. 7 shows another example of comparison between results obtained by He et al.'s work [18] and our algorithm. Fig. 7(e) is the result obtained by [18], which illustrates that the result of this method has color distortions especially in the sky region, and the shore near the horizon is oversaturated. In addition, the buildings near the observer are very dark and lose much detailed information. Notice that our result greatly enhances the visibility of the scene without producing color distortion, thanks to our adjusted transmission map. Moreover, the color of our result is consistent with the original scene.

4.2. Quantitative Evaluation

In this work, we apply the *Image Quality Assessment (IQA)* quality measure, introduced by Aydin et al. [20], to quantitatively assess and evaluate the quality of dehazing techniques. The IQA metric, including a model of the human visual system (HVS), is capable of comparing a pair of images with radically different dynamic ranges. Carefully calibrated and validated through a series of perceptual experiments, the IQA metric can evaluate both the contrast changes and three classes of structural changes yielded by tone mapping operators. The IQA metric classifies the structural changes into three intuitive categories: *loss of visible contrast (green)* - contrast that was visible in the reference image becomes invisible in the transformed image, *amplification of invisible contrast (blue)* - contrast that was invisible in the reference image becomes visible in the transformed image, and *reversal of visible contrast (red)* - contrast that is visible in both reference and transformed images, but with different polarity. Loss of visible contrast (*green*) is relating to image blurring, while contrast amplification (*blue*) and contrast reversal (*red*) are relating to image sharpening.

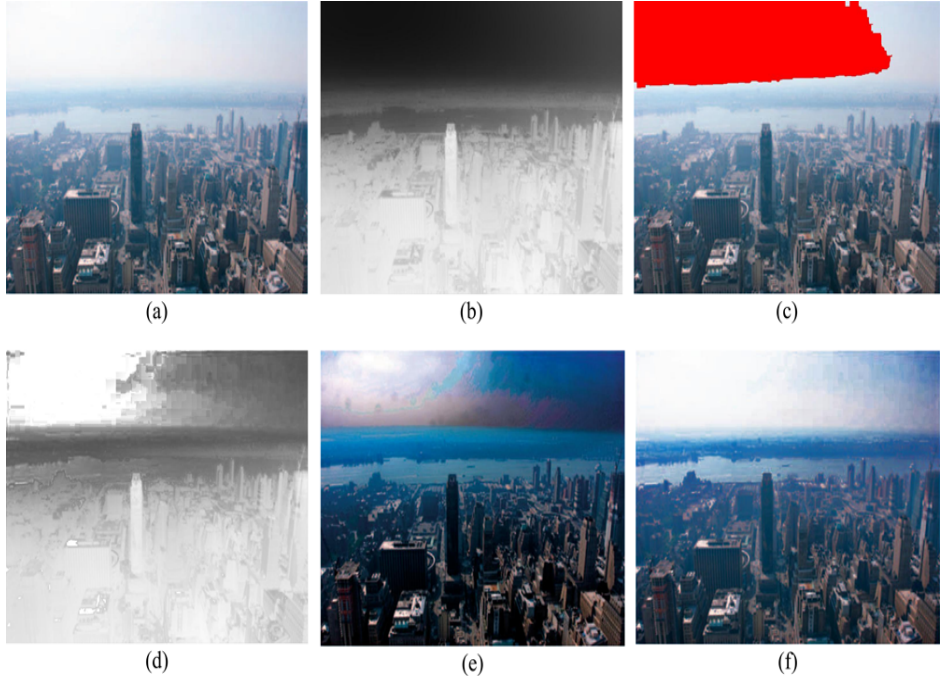


Fig. 7: Comparison with He et al.’s work [18]. (a) Input hazy image. (b) Refined transmission map. (c) Detected sky region. (d) Our adjusted transmission map. (e) He et al.’s result [18]. (f) Our haze removal result.

Fig. 8 shows the comparative results of employing the IQA metric on two input hazy images and their corresponding dehazed results, using the method of Tan [7], Fattal [8], Kopf et al. [19], He et al. [18] and ours. The top-right table of Fig. 8 shows the average comparative ratios of the color pixels obtained by the IQA measure. According to the table, our dehazed results’ loss of visible contrast scored the second best, which means that image blurring caused by our algorithm is less than other three techniques, except for He et al [18]. Since Tan [7] removes the haze effect by maximizing the local contrast of the restored image, it achieved the maximal score in improving contrast. However, the colors of its recovered results (please see Fig. 8(b)) are oversaturated and inconsistent with the scene’s original colors. Compared with other techniques (excluding Tan’s work [7]), our algorithm restores the images with higher contrast.

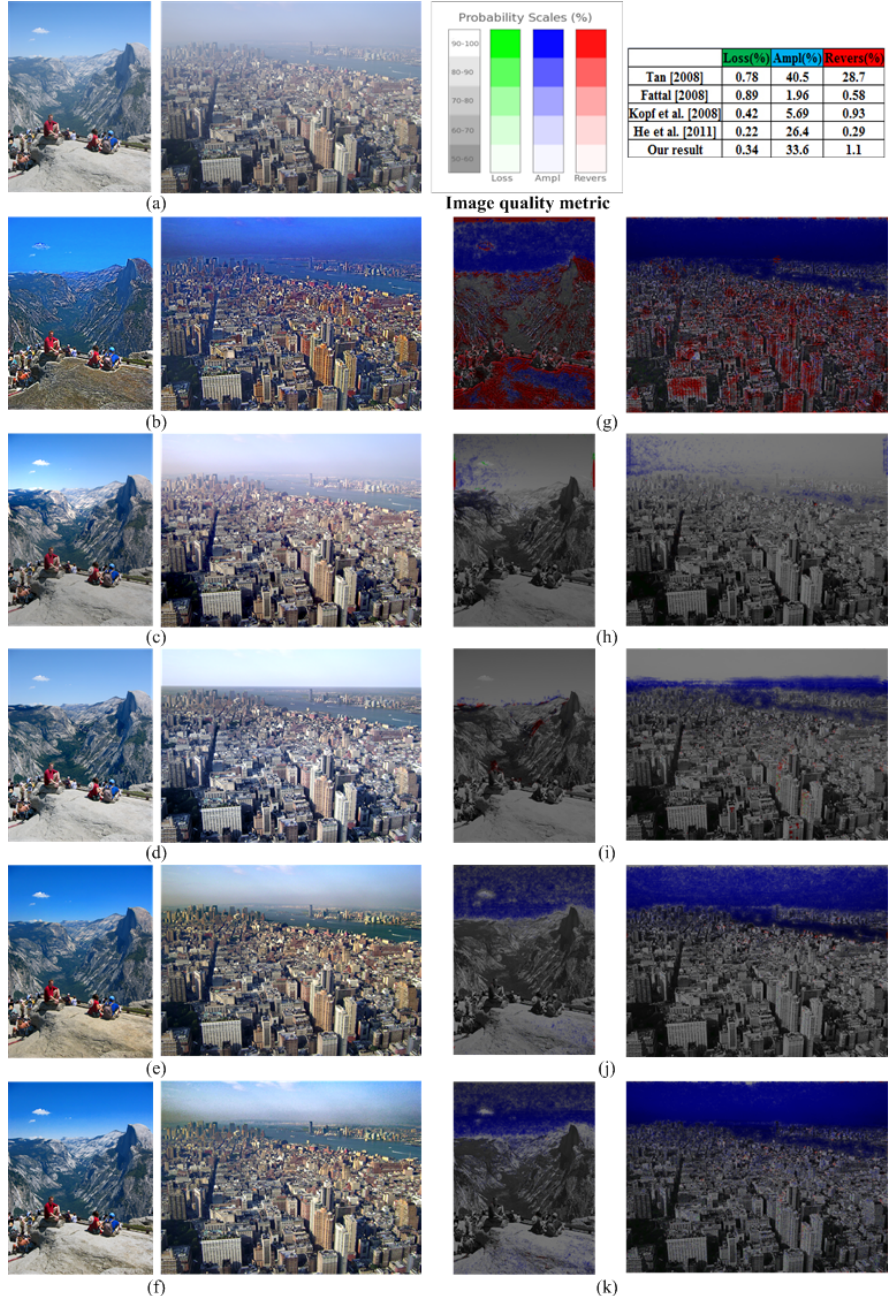


Fig. 8: Evaluation of the recovered results using the IQA metric. (a) Input hazy images. (b) Tan's results [7]. (c) Fattal's results [8]. (d) Kopf et al.'s results [19]. (e) He et al.'s results [18]. (f) Our results. (g), (h), (i), (j), (k) Corresponding IQA metric responses of (b), (c), (d), (e) and (f), respectively.

5. Conclusion and Discussion

In this work, we present an effective and robust method based on dark channel prior for single image dehazing. Our approach is physical valid and can achieve visually compelling results. Meanwhile, the processing speed of our method is fast. Unlike most of previous researches which assume the attenuation coefficient to be constant in homogeneous atmosphere, we give a brief description of the attenuation coefficient which decreases exponentially with respect to the height in inhomogeneous atmosphere. It is more reasonable and comprehensive to the physical interpretation of the attenuation coefficient. In order to avoid color distortion in sky regions similar to the atmospheric light, we first propose a fast and effective way to automatically estimate the rough sky region in the input hazy image. We then adjust the refined transmission map by comparing the average intensity of our detected sky region with the value of the global atmospheric light.

Our proposed algorithm has been tested on a large set of images plagued by haze in natural environment and traffic scene environment. The recovered results contain few block artifacts and halos even in abrupt discontinuities. The color distortion that commonly exists in most sky regions are overcome by our proposed algorithm. Moreover, the results obtained by our proposed approach can maximize the preservation of detail information and are consistent with the original scenes.

However, our proposed algorithm has its limitations as well, which is resulted from our estimated sky regions. When handling with images plagued by very dense haze, our algorithm may lead to a false interpretation of objects shrouded in dense haze as sky regions. Fortunately, our sky detection approach can be applied to most cases.

In the future work, we would like to develop more accurate and robust algorithms for image haze removal and extend our work to the problem of video dehazing.

6. Acknowledgments

The work was supported by the National Natural Science Foundation of China under the Grants 61273245 and 91120301, the 973 Program under the Grant 2010CB327904, the open funding project of State Key Laboratory of Virtual Reality Technology and Systems, Beihang University (Grant No. BUAA-VR-12KF-07), and Program for New Century Excellent Talents in

University of Ministry of Education of China under the Grant NCET-11-0775. The work was also supported by Beijing Key Laboratory of Digital Media, Beihang University, Beijing 100191, P.R. China.

References

References

- [1] J.Y. Chiang and Y.C. Chen, Underwater image enhancement by wavelength compensation and dehazing, IEEE Trans. on Image Processing 21 (4) (2012) 1756-1769.
- [2] S.K. Nayar and S.G. Narasimhan, Vision in bad weather, Proc. ICCV 2 (1999) 820-827.
- [3] S.G. Narasimhan and S.K. Nayar, Chromatic framework for vision in bad weather, Proc. CVPR 1 (2000) 598-605.
- [4] S.G. Narasimhan and S.K. Nayar, Contrast restoration of weather degraded images, IEEE Trans. on Pattern Analysis and Machine Intelligence 25 (6) (2003) 713-724.
- [5] Y.Y. Schechner, S.G. Narasimhan and S.K. Nayar, Instant dehazing of images using polarization, Proc. CVPR 1 (2001) 325-332.
- [6] E. Namer and Y.Y Schechner, Advanced visibility improvement based on polarization filtered images, Optics & Photonics 2005. International Society for Optics and Photonics, 2005.
- [7] R.T. Tan, Visibility in bad weather from a single image, Proc. CVPR, 2008, pp. 1-8.
- [8] R. Fattal, Single image dehazing, ACM Transactions on Graphics (TOG) 27(3) 2008 72:1-72:9.
- [9] K. He, J. Sun, and X. Tang, Single image haze removal using dark channel prior, Proc. CVPR, 2009, pp. 1956-1963.
- [10] S.G. Narasimhan and S.K. Nayar, Vision and the atmosphere, Int'l J.Computer Vision 48 (3) (2002) 233-254.

- [11] J.P. Oakley and B.L. Satherley, Improving image quality in poor visibility conditions using a physical model for contrast degradation, *IEEE Trans. on Image Processing* 7 (2) (1998) 167-179.
- [12] A. J. Preetham, P. Shirley, B. Smits, A practical analytic model for daylight, In *Proceedings of the 26th annual conference on Computer graphics and interactive techniques*, 1999, pp. 91-100.
- [13] K. He, J. Sun, and X. Tang, Guided image filtering, *Proc. ECCV*, 2010, pp. 1-14.
- [14] S.G. Narasimhan and S.K. Nayar, Interactive (de)weathering of an image using physical models, *IEEE Workshop on Color and Photometric Methods in Computer Vision* 6 (6.4) 2003.
- [15] A. Levin, D. Lischinski, and Y. Weiss, A closed form solution to natural image matting, *Proc. ICCV* 1 (2006) 61-68.
- [16] C. Tomasi, R. Manduchi, Bilateral filtering for gray and color images, *Proc. ICCV*, 1998, pp. 839-846.
- [17] N. Draper, H. Smith, *Applied regression analysis* (Second Edition). John Wiley, 1981.
- [18] K. He, J. Sun, and X. Tang, Single image haze removal using dark channel prior, *IEEE Trans. on Pattern Analysis and Machine Intelligence* 33 (12) (2011) 2341-2353.
- [19] J. Kopf, B. Neubert, B. Chen, M. Cohen, D. Cohen-Or, O. Deussen, M. Uyttendaele, and D. Lischinski, Deep photo: model-based photograph enhancement and viewing, *ACM Trans. on Graphics (TOG)* 27 (5) (2008) 116:1-116:10.
- [20] T.O. Aydin, R. Mantiuk, K. Myszkowski, H.P. Seidel, Dynamic range independent image quality assessment, *ACM Trans. on Graphics (TOG)* 27 (3) (2008) 69:1-69:10.